Electron-induced wettability modification

Daniel Aronov, Michel Molotskii, and Gil Rosenman*
Department of Physical Electronics, School of Electrical Engineering, Tel-Aviv University, Tel Aviv 69978, Israel
(Received 4 December 2006; revised manuscript received 13 May 2007; published 27 July 2007)

The pioneering works by Lippmann [Ann. Chim. Phys. **5**, 494 (1875)] and Frumkin [Actual. Sci. Ind. **373**, 5 (1936)] reported on electrowetting phenomenon. It was shown that electric potential, applied to an interface between a conducting liquid droplet and solid surface, strengthened the wetting effect. Here, we describe pronounced decrease of wettability induced by a low-energy electron irradiation. We observe this effect in many materials of different origins. The proposed theory of this phenomenon explains the found growth of the hydrophobicity under an electron irradiation by decreasing solid/liquid and solid/vapor interfacial free energies, when reduction of the latter is always higher. This theory considers the droplet shape dependence on the incident electron charge density and energy of the incident electrons, as well as on the liquid and solid origins. The results of calculations are in a good agreement with the experimental data obtained for water droplet on amorphous silicon dioxide. The effect of the decrease of the wettability, induced by an electron irradiation at low incident charge, is completely reversible after subjection of the electron-irradiated material to ultraviolet illumination, which restores its initial wettability state.

DOI: 10.1103/PhysRevB.76.035437 PACS number(s): 68.35.Md, 81.65.−b, 61.80.Fe

I. INTRODUCTION

Studies of electrocapillarity started in 1875 when Lippmann[1] found a strong variation of an electrolyte droplet shape under an electric potential applied to a solid/liquid interface. In the 1930s, Frumkin[2] used the same idea for the electrowetting phenomenon. He showed that electric charges at a solid/liquid interface modify the contact angle of an electrolyte drop placed on a solid surface. The charges and dipoles were redistributed when an external electric potential was applied between a conducting liquid drop and a metallic electrode, separated by a thin dielectric layer. As a result, an appreciable increase in the wetting was observed.[3,4] The contact angle θ dependence on the applied electric potential may be described within Young's equation,[5]

$$\gamma_{lv} \cos \theta = \gamma_{sv} - \gamma_{sl}, \tag{1}$$

as a result of the reduction of solid/liquid interfacial free energy γ_{sl} under applied potential. Here, the symbol γ refers to the surface interfacial free energies between the phases (solid, liquid, and vapor), indicated by the subscripts. It should be noted that the interfacial free energies related to the solid/vapor γ_{sv} and the liquid/vapor γ_{lv} remain constant and independent from the applied potential.[6,7] The contact angle in Eq. (1) represents the state of the solid/liquid/vapor system that has the minimal Gibbs energy.[8]

We found the opposite phenomenon: a decrease in the wetting of solids due to a low-energy electron irradiation.[9,10] We observed this effect in more than 20 solid materials of different origins, such as *n*- and *p*-Si, SiO_2, S_3N_4, mica, Al_2O_3, glass, Al and Ti metals, which are always coated with oxide films, and biomimetic materials (sea shells, hydroxyapatite,[11] and related calcium phosphates).

Diverse surface modification methods have been used to decrease the wettability of the solid materials.[6,12–17] However, these methods are based on modifying the surface by electrochemical processes[6,12] or radiation-induced damages.[14,15] In our experiments, we took steps to eliminate the contribution of these effects.

In the present work, the experimental results and developed theoretical models of the found decrease of the wetting properties are presented using amorphous SiO_2 as a representative material.

II. EXPERIMENT

A. Materials

In this work, the investigations were carried out on 600 nm thick thermal oxide film grown on the top of a *p*-type Si substrate with resistivity in the range of 11–17 Ω cm. The oxide thickness was controlled by a spectroscopic ellipsometer (M-2000, J.A. Woollam Co., Inc.). The samples were thoroughly cleaned by a standard Radio Corporation of America (RCA) cleaning method using $NH_4OH/H_2O_2/H_2O$ and $HCl/H_2O_2/H_2O$ solutions.[18]

B. Methods

The electron irradiation of the studied SiO_2 samples was performed by a commercially available electron gun (EFG-7, Kimball Physics Inc., USA) in vacuum 10^{-7} Torr at room temperature, using incident electron energy in the range of E_p=10–500 eV. The incident electron charge Q was varied up to 150 $\mu C/cm^2$.

The result of charging was controlled by measuring the induced surface potential φ_s using Kelvin probe force microscopy (KPFM). KPFM is based on modified atomic force microscopy (Multimode DI, USA) operated at room temperature in ambient air. The local topographic and electric potential distributions were measured by Pt/Ir-coated Si tips with diameters of ~30 nm.

The basic measurements of the wettability were performed by controlling the static contact angles of sessile drops of deionized water (*p*H=5.5 and resistivity was more than 17 MΩ cm), placed on a sample surface. Additional

TABLE I. List of used liquids and their surface tensions (Refs. 19 and 20).

	Supplier	purity (%)	Surface tension (mJ/m^2)
n-hexane	Merck	99	18.6
Cyclooctane	Alfa Aesar	99+	29.9
1-bromonaphtalene	Alfa Aesar	97	43.9
Ethylene glycol	Aldrich	99	48.0
Formamide	Alfa Aesar	99.5	57.5
Water		Deionized	72.8

studies were also implemented using some probe liquids such as *n*-hexane, cyclooctane, 1-bromonaphthalene, ethylene glycol, and formamide. Their surface tension varies in a very wide range of 18.6–72.8 mJ/m^2 (Table I). The effect of surface heterogeneity of the studied SiO_2 samples was examined by measuring contact angle hysteresis using the tilting plate technique. The optical wettability inspection was performed by an inspection microscope (Olympus MX-50, Opelco, USA). The volume of the liquid was kept constant (2 μl) all over the contact angle measurements of different specimens. The wettability investigations were carried out with an accuracy of $\pm 1°$ at a temperature of 26 ± 1 °C and a relative humidity (RH) of $(45 \pm 5)\%$.

The wettability modulation was also performed by ultraviolet (UV) illumination using nonfiltered UV light (185–2000 nm). The UV spot light source is equipped with 200 W Hg-Xe lamp (Hamamatsu). The illumination duration was 5 min.

X-ray photoelectron spectroscopy (XPS) was applied to control chemical surface modification of the studied samples after a low-energy electron irradiation. The measurements were performed in ultrahigh vacuum (3×10^{-10} Torr pressure) using 5600 multitechnique system (PHI, USA).

III. RESULTS

Figure 1 shows the variation of the water droplet shape as a result of an electron irradiation of the amorphous SiO_2 substrate. The water repellency of the SiO_2 grows continuously with increasing incident electron charge from the initial hydrophilic (water contact angle of $\theta_0 = 18°$) to pronounced hydrophobic state ($\theta = 89°$). The contact angle hysteresis does not exceed 15° for the hydrophobic state.

Figure 2 presents the graph of the cosine of the water contact angle θ as a function of the absolute value of the incident electron charge Q (incident electron energy is $E_p = 100$ eV). Three strongly different regions can be distinguished at the presented graph. In the first region, which is observed for a low incident charge ($Q < 0.15$ $\mu C/cm^2$), the contact angle increases up to $\theta \sim 33°$. At this stage, charge-induced hydrophobicity variation, $\cos\theta$, is proportional to the charge as Q^2. The second, saturation region ($0.15 < Q < 1$ $\mu C/cm^2$), is characterized by a very weak variation of the contact angle θ. Furthermore, in the third region ($Q > 1$ $\mu C/cm^2$), the contact angle θ continues to increase monotonically and reaches $\theta \sim 89°$. Identical three regions were also observed on the curve of the surface potential difference φ_s versus the incident electron charge Q, measured by KPFM (Fig. 2). Monotonous increase of the surface potential is found in the first region ($Q < 1.5$ $\mu C/cm^2$), which passes to the second one, intermediate region, where the variation of the φ_s value is weak. The third region is characterized by a new stage of continuous fast growth of the surface potential φ_s, reaching its maximum value at $Q \sim 50$ $\mu C/cm^2$. Figure 3 displays a close-up view of the cosine of the water contact angle θ and surface potential φ_s versus the incident charge $Q < 0.25$ $\mu C/cm^2$ (first region). The dotted lines refer to the calculated results, based on the proposed model.

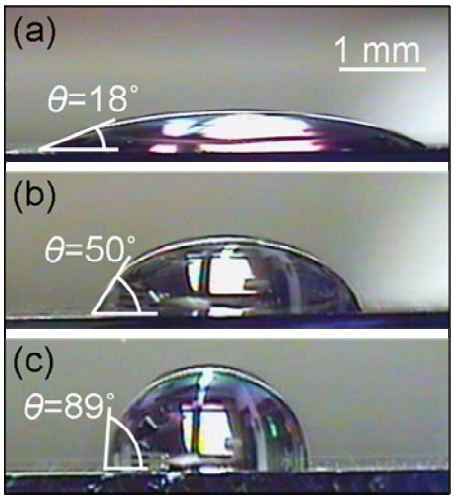

FIG. 1. (Color online) Variation of the water contact angle θ on the SiO_2 surface, induced by a low-energy electron irradiation: (a) initial condition and [(b) and (c)] after the electron irradiation at incident charge density $Q = 1.5$ and 150 $\mu C/cm^2$, respectively. The electron irradiation energy is $E_p = 100$ eV.

Figure 4 shows Zisman plots,[21] constructed for untreated and irradiated SiO_2 surfaces, respectively. The irradiation was performed by applying electron flux with the energy $E_p = 100$ eV and variable incident electron charge $Q = 0.10$

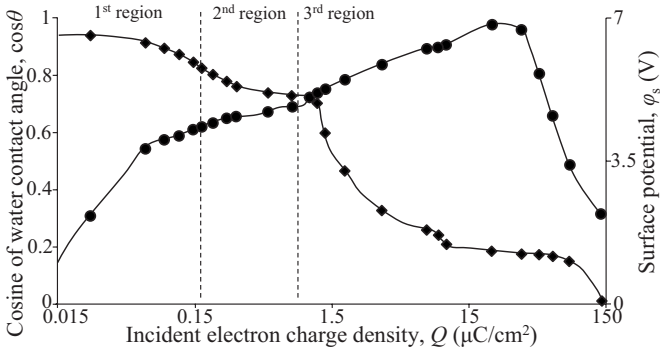

FIG. 2. Dependence of the cosine of the water contact angle θ (squares) and the surface potential φ_s (circles) at the SiO_2 surface on the incident electron charge density Q. The electron irradiation energy is $E_p = 100$ eV.

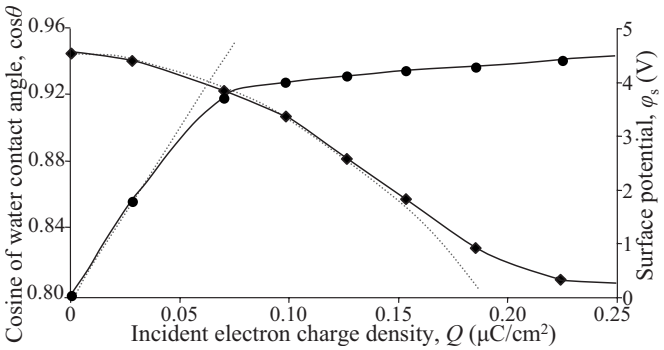

FIG. 3. Close-up of the first region. Dependence of the cosine of the water contact angle θ (squares) at the SiO_2 surface and its surface potential φ_s (circles) on the incident electron charge density Q. Dotted lines show the theoretical approximation dependences. The electron irradiation energy is $E_p=100$ eV.

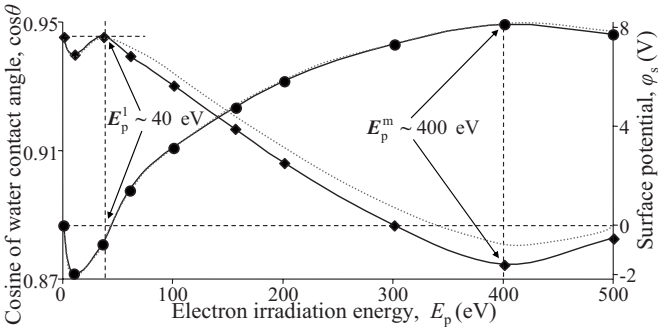

FIG. 5. Dependence of the cosine of the water contact angle θ (squares) and surface potential φ_s (circles) on the electron irradiation energy in an interval of $E_p=10-500$ eV. Dotted lines show the calculated approximation dependence. The incident charge density is $Q=0.05$ $\mu C/cm^2$.

and 0.15 $\mu C/cm^2$ (first region). The data, collected on the SiO_2 surfaces, exhibit the linear relationships between cos θ and liquid surface tensions γ_l, which are listed in Table I.

Figure 5 shows a dependence of the cosine of the water contact angle θ and surface potential φ_s on the energy of the incident electrons E_p, ranging from 0 to 500 eV, while the incident charge Q is invariable for all varieties of energies ($Q=0.05$ $\mu C/cm^2$, which is related to the first region). Measured experimental parameters, cos θ and φ_s versus E_p, demonstrate two different stages. In the range of small energies $E_p<40$ eV, they decrease and then restore their initial values at $E_p\sim40$ eV. The second stage is characterized by a monotonic behavior when both cos θ and φ_s gradually increase, reaching saturation at $E_p\sim400$ eV.

IV. DISCUSSION

A. Chemical contaminations and surface defects

The electron-irradiated SiO_2 samples show a strong variation of the wettability, induced by electron charging (Figs. 1 and 2). The experimental results of measurements of the static contact angle θ and the electric potential φ_s demonstrate three pronounced different stages (Fig. 2), which allow assuming that different physical mechanisms are responsible for the observed behavior of cos θ and φ_s as a function of the incident electron charge Q.

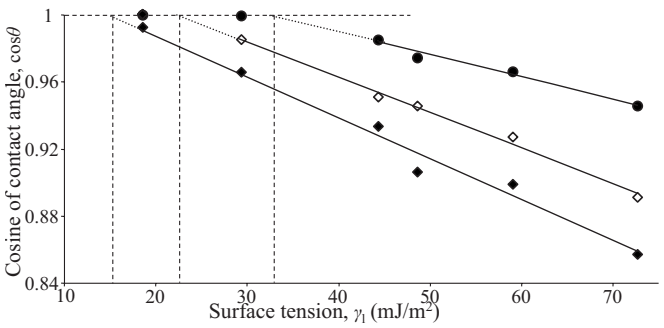

FIG. 4. Relation between the contact angle θ on nonirradiated (circles) and electron-irradiated (squares) SiO_2 surface and the surface tension of various liquids γ_l (Table I). Open and closed squares refer to irradiation with the incident charge density of $Q=0.10$ and 0.15 $\mu C/cm^2$, respectively.

An electron irradiation of a solid surface may lead to various surface modifications such as chemical modification, defect generation, and electrical charging. Chemical contaminations of the electron-treated samples in each region were inspected by the XPS measurements of the irradiated SiO_2 samples. The results showed negligible changes in chemical identity in the first and second regions (Fig. 2), whereas in the third region (Fig. 2) significant new chemical contaminations were found. The XPS measurements clearly demonstrated the formation of alkyl groups (CH) on the SiO_2 surface in the third region. The alkyl groups are known to be strongly hydrophobic.[22] These organic compounds may be used as surface passivation layers for Si-based materials.[23] Thus, the observed growth of the water contact angle θ in the third region (Fig. 2), in addition to the reduction of the surface potential φ_s (Fig. 2), may be ascribed to these surface chemical identity changes. It should be noted that definite concentrations of carbon were found in all studied samples before the electron treatment.

The observed effect of the decrease of the wettability may be referred to surface structural changes, induced by electronic irradiation. Generation of new surface defects is a possible mechanism for such structural modification. As is known,[24–26] surface defects may play a role of the active chemical centers and influence the wettability. However, generation of the defects at the SiO_2 surface starts from the threshold electron energy $E_{th}=500$ eV.[27] Therefore, in order to exclude the contribution of the radiation-induced defects, all the experiments in this paper were carried out below this threshold, at $E_p<E_{th}$.

The experimental data (Figs. 2 and 3) and the surface chemical identity studies show distinctly that the wettability variations observed in the first and the third regions governed by quite different physical mechanisms, whereas the second region may be referred to the intermediate regime where the governed mechanisms for the first and third region are changed. A monotonic increase in the contact angle θ observed in the first region is accompanied by a pronounced variation of the surface electric potential φ_s (Fig. 2). The

linear growth of the φ_s value in this region allows assuming that the found decrease of the wettability in the first region is directly related to electrical charging. It should be reminded that no variation in surface chemical composition was found in the first region.

Moreover, it is also impossible to refer a growth of water repellency to charging of already existing surface defects. Such defects may induce strong electrostatic interactions with dipole water molecules and play a role of hydrophilic adsorption sites on the silica surface.[28,29] Therefore, capture of carriers on surface traps should lead to an increase of the wettability, while the opposite effect is observed (Figs. 1 and 2). In addition, at the low values of Q, the concentration of surface-active centers and the interphase energy proportional to them should be changed linearly with Q. Hence, in accordance with Eq. (1), the cosine of the contact angle θ should also be changed linearly with Q. However, the observable square-law dependence of the effect of the decrease of the wettability on the charge density Q specifies the absence of some appreciable contribution of radiation-induced active centers (Figs. 2 and 3). The number of new charged surface centers, appearing under an electron irradiation, is small and their contribution to the process is negligible. Evidence of validity of this assumption is the fact that the existing theory of dielectric charging by an electron irradiation that dose not consider a possibility of carrier capturing on a surface is in good agreement with experimental data.[31–35]

B. Origin of the wettability decreasing effect in the first region

Our approach is based on the electrowetting effect that occurs under electric field generated by electric charge captured near the surface. It should be marked that the main difference from the conventional electrowetting effect[3,4] is that the electron irradiation of the material surface leads not only to variation of the solid/liquid interface but also to variation of the solid/vapor interface. In accordance with Eq. (1), one may assume that the observed charge-induced effect of the decrease of the wettability in the first region (Fig. 3) may be explained by supposing that the reduction of γ_{sv} exceeds the reduction of γ_{sl} ($\Delta\gamma_{sv} > \Delta\gamma_{sl}$) under an electron irradiation. It will be shown below that this condition is really met for any liquid, in which molecules do not exhibit strong chemical interactions with charged centers, appearing on the electron-irradiated surface.

In addition, critical surface tensions of untreated and electron-irradiated samples were compared (Fig. 4) using the method of the so-called "Zisman plot," developed in Ref. 21. The authors of Ref. 21 introduced the concept of critical surface tension γ_c as an empirical method of determining the "wettability" of solid surfaces by plotting the cosine of the contact angle θ versus the surface tensions γ_l of various liquids with known surface tension values (Table I). The critical surface tension of a solid surface γ_c is defined as the x intercept of the $\cos\theta(\gamma_c)$ curve at $\cos\theta=1$. Physically, γ_c separates the liquids that form zero contact angles on the solid surface (i.e., spread spontaneously) from those that form higher contact angles and do not spread. The critical surface tension seems to be a basic property of the solid alone. Figure 4 illustrates the Zisman plot; the dependence of the contact angle on the surface liquid tensions, $\cos\theta(\gamma_c)$. The measurements were performed using the various liquids (Table I) on nonirradiated (circles) and electron-irradiated (squares) SiO_2 surfaces. The irradiation was performed by electrons with $E_p=100$ eV and variable incident electron charge from $Q=0.10$ to 0.15 $\mu C/cm^2$, which is related to the first region (Fig. 3). The obtained data (Fig. 4) distinctly show that the low-energy electron irradiation leads to a significant decrease of the critical surface tension γ_c of the SiO_2 surface. It should be noted that the observed values of the critical surface tension for the untreated SiO_2 are in good agreement with the known data for the native thermal oxide ($\gamma_c = 27-42$ mJ/m^2).[30]

1. Electron-irradiation-induced solid/vapor and solid/liquid interfacial free energy variation

The process of dielectric charging induced by an electron irradiation includes several stages.[31–35] If E_{eh} is the mean energy required for creation of electron-hole pairs, then every incident electron excites about $\sim E_p/E_{eh}$ electron-hole pairs. Heavy and weak mobile holes are almost instantly trapped by the numerous traps in amorphous dielectrics. The electron mobility in amorphous materials is by several orders of magnitude higher than that of the holes.[36,37] Therefore, the excited secondary electrons should penetrate deeper than holes into the dielectric bulk. As a result, the generated and trapped electron and hole charges have a double-layer structure. The positive charge is formed by the localized holes in the vicinity of the surface, whereas the negative charge is created by the trapped electrons at the bulk levels far from the surface. A lifetime of localized carriers of charge strongly depends on the energy spectrum of traps in the energy gap of the SiO_2. It has been shown that the amorphous SiO_2 possesses very deep electron and hole traps with energy depth, reaching 2.2–2.5 eV.[38,39] Thermal ionization of such traps is practically impossible at room temperature, since the estimated ionization time exceeds 10^{22} s that follows from the expressions given in Ref. 40. Certainly, there are other possible mechanisms for the deep trap ionization, which are not related to thermionic ionization of the carriers to the bulk band states, for instance, the tunneling recombination of electrons and holes, the recombination of localized carriers with mobile charged defects of an opposite sign, etc. However, such processes are also very inefficient, and therefore trapped carriers have a long lifetime. Experimental studies showed that the deep traps are stable in the SiO_2 at least 3 years at room temperature.[41,42] Time duration in our experiments, including exposure time of the electron irradiation and time for the contact angles measurements, did not exceed a couple of hours. Therefore, the charge value and distribution stay invariable during the experiment, and the studied system is under quasiequilibrium state.

The charge distribution $\rho=\rho_e+\rho_h$ refers to the distribution of the bulk density of the electron ρ_e and hole ρ_h charges. The potential $\varphi=\varphi_0+\varphi^*$ inside a dielectric consists of the potential φ_0 of the real charge ρ in an infinite sample and the potential φ^* of an image charge. Hence, the surface free energy density variation as a result of the dielectric charging

may also be expressed as a sum of two terms:

$$\Delta\gamma = \Delta\gamma_0 + \Delta\gamma^*,$$

where

$$\Delta\gamma_0 = \frac{1}{2}\int \rho(x)\phi_0(x)dx$$

and

$$\Delta\gamma^* = \int \rho(x)\phi^*(x)dx. \quad (2)$$

Here, $\Delta\gamma_0$ is the self-energy of the charge ρ in an infinite sample and $\Delta\gamma^*$ is the energy of the interaction between real charge ρ and its image. It is known that the presence of a net electric charge at the solid/liquid interface reduces the interfacial free energy γ_{sl},[3,4] in the case of positive self-energy of the charges, i.e., when the main contribution is defined by repulsion between like charges. Moreover, the solid/vapor interface free energy γ_{sv} is also reduced as a result of a low-energy electron irradiation that is consistent with the Zisman plot measurements carried out on untreated and charged SiO_2 surface (Fig. 4). All these statements are in accordance with the work of Gibbs[8] and its detailed analysis by Rice.[43]

The presence of a net electric charge at the interface reduces interfacial free energies γ by the order of the charge energy density $\Delta\gamma$ at this interface. Both the solid/vapor and the solid/liquid interface free energies decrease up to

$$\gamma_{sv} = \gamma_{sv}^0 - \Delta\gamma_0 - \Delta\gamma_{sv}^*,$$

$$\gamma_{sl} = \gamma_{sl}^0 - \Delta\gamma_0 - \Delta\gamma_{sl}^*, \quad (3)$$

as a result of the electron irradiation followed by charging. Here, γ_{sv}^0 and γ_{sl}^0 are the initial values of the interfacial free energies before charging. Equation (3) will be generalized below to include liquid electrostatic energy contribution to solid/electrolyte interfacial free energy under an electron irradiation.

The positive energy $\Delta\gamma_0$ does not depend on the environmental conditions at the interfaces (charged dielectric/liquid and dielectric/vapor) and leads to uniform variation of the surface tension of irradiated dielectric. In such a way, $\Delta\gamma_0$ is not capable of influencing material wettability due to its constant value for both the solid/vapor and the solid/liquid interfaces. The contribution of the value of this energy to Young's equation [Eq. (1)] is canceled and does not influence the wettability. Due to the same reason, the sign of the $\Delta\gamma_0$ is not able to influence the wettability variation under irradiation. The effect of the decrease of the wettability under an electron irradiation is caused only by the electrostatic energy term $\Delta\gamma^*$, related to the interactions of an excess charge with its images, which strongly depends on the environmental conditions.

For determination of the value of the energy $\Delta\gamma^*$, the irradiation-induced charge distributions, ρ_e and ρ_h, are approximated by simple exponential functions:

$$\rho_e(x) = \rho_e^0 e^{-x/R_e},$$

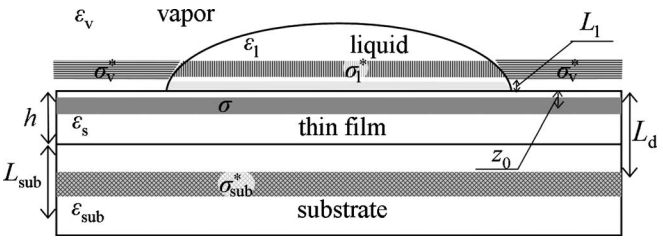

FIG. 6. Sketch illustrating the geometry of the various layers including their dielectric constants and the position of the excess charge σ and its image σ^*. In thin films ($h \ll L_f$), the image charge σ^* is formed in the liquid (σ_l^*) and vapor (σ_v^*) environment and substrate (σ_{sub}^*).

$$\rho_h(x) = \rho_h^0 e^{-x/R_h}, \quad (4)$$

where

$$\rho_e^0 = -\frac{\left[(1-\eta)\left(1+\frac{E_p}{E_{eh}}\right)-\delta\right]Q}{R_e},$$

$$\rho_h^0 = \frac{(1-\eta)E_p Q}{E_{eh}R_h}. \quad (5)$$

Here η and δ are the backscattering and the secondary electron emission coefficients, respectively, and R_e and R_h are the electron and the hole average penetration depths into the sample. Thus, the surface charge density σ, under an electron irradiation, is expressed by

$$\sigma = \rho_e^0 R_e + \rho_h^0 R_h = (\chi - 1)Q. \quad (6)$$

Here, χ is the total emission coefficient:

$$\chi = \eta + \delta. \quad (7)$$

The nature of the interactions of the excess charge σ with the image charges σ^* is dependent on the relation between the screening length L_f in the dielectric film and its thickness h. In thin films ($h \ll L_f$, Fig. 6) the image charge σ^* is formed in liquid (σ_l^*) and vapor (σ_v^*) environment and substrate (σ_{sub}^*), while in thick films ($h \gg L_f$, Fig. 7) the substrate contribution is screened by mobile carriers ($\sigma_{sub}^*=0$). We will determine the expression of the interaction energy $\Delta\gamma^*$ in both cases.

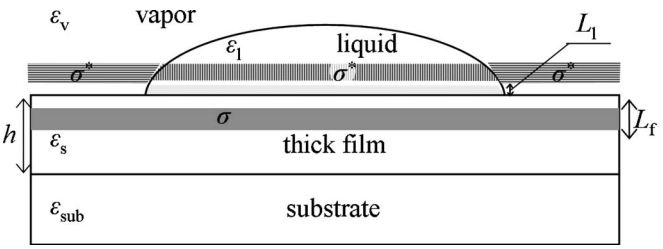

FIG. 7. Sketch illustrating the geometry of the various layers including their dielectric constants and the position of the excess charge σ and its image σ^*. In thick films ($h \gg L_f$), the image charge σ^* is formed only in the liquid (σ_l^*) and vapor (σ_v^*) environment.

2. Wetting of thin films

Let us consider the energy of the image in thin dielectric film, which is located between the substrate and the environment (Fig. 6). Following the fact that the strength of the electric field produced by a charged plate does not depend on a distance from the charge σ, the value of the image charges σ^* is not dependent on the distribution of real charge inside the film, but is determined only by the value of the excess charge σ [Eq. (6)]. We consider the plate charge σ placed at a distance z_0 from the interface film/environment (Fig. 6). It will be shown below that the obtained results are not dependent on the value z_0.

For the calculation of the field E_z of the charge σ, the known expression for the normal components of the field of the point charge q is used (see, for example, Ref. 44):

$$E_z(\rho,z) = \frac{2q}{\varepsilon_m+\varepsilon_s}\left(\int_0^\infty \frac{kJ_0(k\rho)e^{-kz}}{1-\beta e^{-2kh}}dk + \frac{\varepsilon_{\text{sub}}-\varepsilon_s}{\varepsilon_{\text{sub}}+\varepsilon_s}\int_0^\infty \frac{kJ_0(k\rho)e^{k[z-2(h-z_0)]}}{1-\beta e^{-2kh}}dk\right), \quad (8)$$

where ρ and z are the cylindrical coordinates, and ε_s, ε_{sub}, and ε_m are the dielectric constants of the dielectric film, substrate, and environment, respectively. Here, $J_0(x)$ is the zeroth-order Bessel function of the first kind and β is the constant that is defined as

$$\beta = \frac{(\varepsilon_m-\varepsilon_s)(\varepsilon_{\text{sub}}-\varepsilon_s)}{(\varepsilon_m+\varepsilon_s)(\varepsilon_{\text{sub}}+\varepsilon_s)}.$$

The denominator of the underintegral functions in Eq. (8) may be specified as a row of βe^{-2kh} functions:

$$\frac{1}{1-\beta e^{-2kh}} = \sum_{n=0}^{\infty}\beta^n e^{-2nkh}.$$

The obtained row can be integrated term by term by taking into account[45] that for $x>0$,

$$\int_0^\infty kJ_0(k\rho)e^{-kx}dk = \frac{x}{(\rho^2+x^2)^{3/2}}.$$

Now, q may be replaced by $dq=2\pi\sigma\rho d\rho$ and the expressions obtained in Eq. (8) may be integrated along the charged plane. The integrals, which do not depend on x, may be written as

$$\int_0^\infty \frac{x\rho d\rho}{(\rho^2+x^2)^{3/2}} = 1.$$

In our case, $x=z$, $2h-z$, and $2(h-z_0)-z$, hence, no dependence on z, z_0, and h is found in the final expression of the field strength. The full field E_f in the dielectric is

$$E_f = \frac{4\pi\sigma}{\varepsilon_m+\varepsilon_s}\left(1+\frac{\varepsilon_{\text{sub}}-\varepsilon_s}{\varepsilon_{\text{sub}}+\varepsilon_s}\right)\sum_{n=0}^{\infty}\beta^n.$$

Since

$$\sum_{n=0}^{\infty}\beta^n = \frac{1}{1-\beta},$$

the final expression for E_f may be formulated as

$$E_f = \frac{4\pi\sigma}{\varepsilon_s}\frac{\varepsilon_{\text{sub}}}{\varepsilon_{\text{sub}}+\varepsilon_m}.$$

and the field E_s of the real charge σ in infinite media with dielectric permittivity ε_s is equal to

$$E_s = \frac{2\pi\sigma}{\varepsilon_s}.$$

Thus, the expression of the field E^*, created by the image charges σ^*, in the film may be written by subtracting E_f from E_s:

$$E^* = E_f - E_s = \frac{2\pi\sigma}{\varepsilon_s}\frac{\varepsilon_{\text{sub}}-\varepsilon_m}{\varepsilon_{\text{sub}}+\varepsilon_m}. \quad (9)$$

The potential φ^* of the field E^* inside the film is given by

$$\varphi^* = \frac{2\pi\sigma}{\varepsilon_s}\left(\frac{\varepsilon_{\text{sub}}-\varepsilon_m}{\varepsilon_{\text{sub}}+\varepsilon_m}\right)(L_d-x), \quad (10)$$

where L_d is the distance from a surface for which the potential becomes zero (Fig. 6). If the dielectric film is located on a metal substrate, l_d is equal to the thickness h of the film. In our case, the dielectric film is deposited on the Si-semiconductor substrate, providing partial penetration of the electric field. The total length L_d of the penetration of the electric field into the Si substrate is

$$L_d = h + \frac{\varepsilon_s}{\varepsilon_{\text{sub}}}L_{\text{sub}}, \quad (11)$$

where l_{sub} is the screening length inside the Si substrate (Fig. 6). For p-type Si with resistivity of 11–17 Ω cm and the dielectric constant of $\varepsilon_{\text{sub}}=11.7$, the Debye screening length[46] is $L_{\text{sub}}\sim 120$ nm at room temperature. In our case, by substituting $h=600$ nm and $\varepsilon_s=3.8$ (Ref. 34) into Eq. (11), the full length is $L_d=640$ nm.

Thus, the expression of the energy $\Delta\gamma^*$ may be obtained by combining Eqs. (2), (4), and (10):

$$\Delta\gamma^* = \frac{2\pi\sigma}{\varepsilon_s}\left(\frac{\varepsilon_{\text{sub}}-\varepsilon_m}{\varepsilon_{\text{sub}}+\varepsilon_m}\right)F_{eh}, \quad (12)$$

where

$$F_{eh} = L_d[\rho_e^0 R_e(1-e^{-L_d/R_e}) + \rho_h^0 R_h(1-e^{-L_d/R_h})] - \rho_e^0 R_e^2\left[1-\left(1+\frac{L_d}{R_e}\right)e^{-L_d/R_e}\right] - \rho_h^0 R_h^2\left[1-\left(1+\frac{L_d}{R_h}\right)e^{-L_d/R_h}\right].$$

It may be assumed for low-energy electrons that $L_d \gg R_e > R_h$. Therefore, Eq. (12) may be simplified to

$$\Delta\gamma^* = \frac{2\pi\sigma^2 L_d}{\varepsilon_s}\left(\frac{\varepsilon_{\text{sub}} - \varepsilon_m}{\varepsilon_{\text{sub}} + \varepsilon_m}\right). \tag{13}$$

Equation (13) describes the variation of the surface free energy as a result of charging and shows that $\Delta\gamma^*$ can acquire positive or negative value, depending on the ratio of the dielectric constants ε_{sub} and ε_m. The value of the energy is positive when the permittivity of a dielectric environment, outside a solid material, is less than that of the substrate ($\varepsilon_m < \varepsilon_{\text{sub}}$). Such situation occurs, for example, on the solid/air interface because the permeability of air $\varepsilon_v \sim 1$ is less than the dielectric permeability of Si $\varepsilon_{\text{sub}}=11.7$. There is an opposite situation on the solid/water interface, when the permeability of water $\varepsilon_l=80.4 \gg \varepsilon_{\text{sub}}=11.7$. Moreover, the dielectric constant of every liquid ε_l exceeds the dielectric constant of the air vapor $\varepsilon_v \sim 1$. As a result, $\Delta\gamma_{sv}^*$ always exceeds $\Delta\gamma_{sl}^*$ [Eq. (13)]. From Eqs. (1) and (3), it is seen that such behavior of the energies $\Delta\gamma_{sv}^*$ and $\Delta\gamma_{sl}^*$ should lead to an increase in the contact angle θ for any liquids.

It should be mentioned that the influence of dielectric properties of an environment on the electrostatic component of the surface tension was known earlier. For example, in accordance with the theory of Onsager and Samaras,[47] the contribution of ions in the electrolyte on surface tension is defined by their interactions with the image charges. Thus, the term of the electrostatic contribution to the electrolyte surface tension should change the sign at transition from the environment with a lower dielectric constant to the environment with a higher dielectric constant in comparison to that of the electrolyte.

3. Liquid electrostatic energy contribution to solid/electrolyte interfacial free energy

The free energy variation $\Delta\gamma_{sl}$ on the solid/liquid interphase induced by an electric charging includes not only the self-energy of the charged dielectric but also the energy of the liquid. The Gouy-Chapman model of an electrolyte in the absence of specific adsorption, in which ions of one sign are kept by a surface more strongly than ions of another sign, has been widely used. Close to the interface, a diffuse double layer is created (Figs. 6 and 7). One of the double-layer plates is the excess charge σ, induced by an electron beam irradiation on a dielectric surface. Another plate is created by ions of the opposite sign, attracted from the electrolyte by the field of charge σ. The increase in the concentration of ions in the electrolyte near the interface leads to the growth of the lateral Coulomb repulsion forces, resulting in additional wetting of the surface, i.e., to an increase in the wettability.

Let us define the diffuse-double-layer energy contribution to the solid/electrolyte interface free energy. In the absence of specific adsorption, the diffusion layer is located at the interface between the liquid and the dielectric surface (Figs. 6 and 7). The total field on the interface E_{int} includes the field $E_\sigma(0)$ of the excess charge σ,

$$E_\sigma(0) = \frac{4\pi\sigma}{\varepsilon_m}\frac{\varepsilon_{\text{sub}}}{\varepsilon_{\text{sub}} + \varepsilon_m},$$

and field equal to $E_\sigma(0)$, created in diffusion layer of an electrolyte by the ions of an opposite sign. Thus, the total field E_{int} on interface may be formulated as

$$E_{\text{int}} = \frac{8\pi\sigma}{\varepsilon_m}\frac{\varepsilon_{\text{sub}}}{\varepsilon_{\text{sub}} + \varepsilon_m}.$$

In the Debye-Hückel approximation, the strength of total field inside the electrolyte is decreasing exponentially with the distance x from the interface:

$$E(x) = E_{\text{int}} e^{-x/L_l},$$

where L_l is the Debye length in the droplet (Figs. 6 and 7) that is given by

$$L_l = \sqrt{\frac{\varepsilon_l kT}{8\pi n_0 e^2 v^2}}. \tag{14}$$

Here, n_0 is the density of the positive or negative ions far from the interface, k is the Boltzmann constant, T is the temperature, e is the electron charge, v is their valences, and ε_l is the electrolyte dielectric constant. Now, the screening charge distribution in an electrolyte may be expressed as

$$\rho(x) = \frac{\varepsilon_l}{4\pi}\frac{dE(x)}{dx} = -\frac{\varepsilon_l E_{\text{int}}}{4\pi L_l} e^{-x/L_l}, \tag{15}$$

and the potential is

$$\varphi(x) = -\int E(x)dx = E_{\text{int}} L_l e^{-x/L_l}. \tag{16}$$

Equation (16) satisfies the boundary condition $\varphi(\infty)=0$.

Equations (15) and (16) allow us to define the expression of the electrostatic contribution to the solid/liquid interface free energy of the diffuse double layer of an electrolyte (G_s):

$$G_s = \int_0^\infty \rho(x)\varphi(x)dx = -\frac{8\pi\sigma^2 L_l}{\varepsilon_l}\left(\frac{\varepsilon_{\text{sub}}}{\varepsilon_{\text{sub}} + \varepsilon_l}\right)^2. \tag{17}$$

It is clearly seen that this contribution has a negative sign ($G_s < 0$). Taking into consideration the Coulomb interactions of charges (the energy $\Delta\gamma_0$), the interaction of an excess charge σ with its image outside the solid (energy $\Delta\gamma^*$), and the electrostatic electrolyte energy G_s, and by combining Eqs. (3), (13), and (17), the solid/vapor interface free energy, induced by the charging effect, is equal to Eq. (3),

$$\gamma_{sv} = \gamma_{sv}^0 - \Delta\gamma_0 - \Delta\gamma_{sv}^* = \gamma_{sv}^0 - \Delta\gamma_0 - \frac{2\pi\sigma^2 L_d}{\varepsilon_s}\left(\frac{\varepsilon_{\text{sub}} - \varepsilon_v}{\varepsilon_{\text{sub}} + \varepsilon_v}\right), \tag{18}$$

whereas the solid/liquid interface γ_{sl} is given by

$$\gamma_{sl} = \gamma_{sl}^0 - \Delta\gamma_0 - \Delta\gamma_{sl}^* + G_s = \gamma_{sl}^0 - \Delta\gamma_0 - \frac{2\pi\sigma^2 L_d}{\varepsilon_s}\left(\frac{\varepsilon_{\text{sub}} - \varepsilon_l}{\varepsilon_{\text{sub}} + \varepsilon_l}\right) - \frac{8\pi\sigma^2 L_l}{\varepsilon_l}\left(\frac{\varepsilon_{\text{sub}}}{\varepsilon_{\text{sub}} + \varepsilon_l}\right)^2. \tag{19}$$

Taking into account expressions (18) and (19), Young's equation may be modified as

$$\gamma_{lv}(\cos\theta_0 - \cos\theta) = \Delta\gamma_{sv}^* - \Delta\gamma_{sl}^* + G_s. \tag{20}$$

In the absence of the irradiation ($\Delta\gamma_{sv}^* = \Delta\gamma_{sl}^* = G_s = 0$), Eq. (20) transforms to the well-known Young's equation for un-

charged surface [Eq. (1)]. As a result of the irradiation, the energies $\Delta\gamma_{sv}^{*}$, $\Delta\gamma_{sl}^{*}$, and G_s are not equal to zero, and so Eq. (20) may be expressed as

$$\gamma_{lv}(\cos\theta_0-\cos\theta)=\frac{2\pi\sigma^2L_d}{\varepsilon_s}\left(\frac{\varepsilon_{\text{sub}}-\varepsilon_v}{\varepsilon_{\text{sub}}+\varepsilon_v}-\frac{\varepsilon_{\text{sub}}-\varepsilon_l}{\varepsilon_{\text{sub}}+\varepsilon_l}\right)-\frac{8\pi\sigma^2L_l}{\varepsilon_l}\left(\frac{\varepsilon_{\text{sub}}}{\varepsilon_{\text{sub}}+\varepsilon_l}\right)^2. \quad (21)$$

It is clear from Eq. (21) that there are two opposite tendencies in the variation of the wettability, induced by an electron irradiation. One of them, which is described by the first term in Eq. (21), relates to the decrease of the wettability, while the other one, which is described by the second term, relates to the increase of the wettability.

If the charge σ is distributed in the vicinity of the dielectric surface, on which the water droplet is placed, the contribution of the last term in Eq. (21) is negligible in comparison to that of the first term. The conditions of our experiments, under an electron irradiation, are $\varepsilon_s=3.8$,[34] $\varepsilon_v=1$, $\varepsilon_{\text{sub}}=11.7$, and $L_d=640$ nm [Eq. (11)]. The deionized water ($\varepsilon_l=80.4$) with ion concentration $n_0\sim5\times10^{14}$ cm^{-3} was used, resulting in $L_l\sim300$ nm [Eq. (14)]. Thus, the relation of the second to the first term is about 10^{-3}. Therefore, in our case, the contribution of the G_s energy to the interface free energy may be neglected. In such a way, Eq. (21) may be expressed as

$$\gamma_{lv}(\cos\theta_0-\cos\theta)=\frac{2\pi\sigma^2L_d}{\varepsilon_s}\left(\frac{\varepsilon_{\text{sub}}-\varepsilon_v}{\varepsilon_{\text{sub}}+\varepsilon_v}-\frac{\varepsilon_{\text{sub}}-\varepsilon_l}{\varepsilon_{\text{sub}}+\varepsilon_l}\right), \quad (22)$$

which describes the effect of the decrease of the wettability or, in the other words, the increase of the water contact angle θ due to irradiation (Fig. 3). It is clearly seen from Eq. (22) that the effect of the decrease of the wettability is due to a difference in energies of the interactions between the excess charge σ and its images on the solid/vapor (σ_s^{*}) and solid/liquid (σ_l^{*}) interfaces. If permeability of the environment ε_v will coincide with ε_l, the effect of the decrease of the wettability will disappear.

4. Wetting of thick films

In the case of thick films, the expression for the field of the image charge σ^{*} [Eq. (9)] should be modified. It was shown above that this field determines the decrease of the wettability under irradiation. For thick films, there is no contribution of the image charge σ_{sub}^{*}, located on a dielectric film/substrate interface, and it is in contrast to thin film case (Figs. 6 and 7). Thus, the irradiated sample can be considered as semi-infinite.

The intensity of the electric field E_0 in the infinite medium, outside the charge σ, located in the vicinity of the dielectric surface (Fig. 7) and creates this field, is equal to

$$E_0=\frac{2\pi\sigma}{\varepsilon_s}.$$

On the other hand, if the charge σ is located in the vicinity of the interface with the dielectric permeability ε_m, then the created image charge $\sigma_m^{*}=\sigma^{*}$ (Fig. 7) is given by

$$\sigma^{*}=\sigma\frac{\varepsilon_s-\varepsilon_m}{\varepsilon_s+\varepsilon_m}.$$

The image charge σ^{*} produces the uniform electric field E^{*} in the charged dielectric,

$$E^{*}=\frac{2\pi\sigma}{\varepsilon_s}\left(\frac{\varepsilon_s-\varepsilon_m}{\varepsilon_s+\varepsilon_m}\right),$$

and potential,

$$\varphi^{*}(x)=\frac{2\pi\sigma L_f}{\varepsilon_s}\left(\frac{\varepsilon_s-\varepsilon_m}{\varepsilon_s+\varepsilon_m}\right)e^{-x/L_f}, \quad (23)$$

which decays exponentially with L_f (Fig. 7). The expression for the energy $\Delta\gamma^{*}$ of the interactions between the excess charge σ and its image σ^{*} can be obtained by combining Eqs. (2), (4), and (23):

$$\Delta\gamma^{*}=\frac{2\pi\sigma L_f^2}{\varepsilon_s}\left(\frac{\varepsilon_s-\varepsilon_m}{\varepsilon_s+\varepsilon_m}\right)\left(\frac{\rho_e^0R_e}{L_f+R_e}+\frac{\rho_h^0R_h}{L_f+R_h}\right). \quad (24)$$

By assuming $L_f\gg R_e$, R_h and using Eq. (6), Eq. (24) may be simplified to

$$\Delta\gamma^{*}=\frac{2\pi\sigma^2L_f}{\varepsilon_s}\left(\frac{\varepsilon_s-\varepsilon_m}{\varepsilon_s+\varepsilon_m}\right). \quad (25)$$

In this case, the total field E_{int}^{sl} on the solid/electrolyte interface is equal to

$$E_{\text{int}}^{sl}=\frac{8\pi\sigma}{\varepsilon_s+\varepsilon_l}.$$

The field inside the electrolyte is given by

$$E(x)=E_{\text{int}}^{sl}e^{-x/L_l}.$$

The screening charge distribution in an electrolyte may be written as

$$\rho(x)=-\frac{\varepsilon_lE_{\text{int}}^{sl}}{4\pi L_l}e^{-x/L_l}. \quad (26)$$

Thus, the potential of this charge becomes

$$\varphi(x)=E_{\text{int}}^{sl}L_le^{-x/L_l}. \quad (27)$$

The electrolyte electrostatic energy G_s contribution to the solid/liquid interface free energy may be expressed, using Eqs. (26) and (27), as

$$G_s=\int_0^{\infty}\rho(x)\varphi(x)dx=-8\pi\sigma^2\varepsilon_lL_l\left(\frac{1}{\varepsilon_s+\varepsilon_l}\right)^2. \quad (28)$$

The solid/vapor interface free energy γ_{sv}, induced by the charging effect, is obtained by introducing Eq. (25) into Eq. (3):

$$\gamma_{sv} = \gamma_{sv}^0 - \Delta\gamma_0 - \Delta\gamma_{sv}^* = \gamma_{sv}^0 - \Delta\gamma_0 - \frac{2\pi\sigma^2 L_f}{\varepsilon_s}\left(\frac{\varepsilon_s - \varepsilon_v}{\varepsilon_s + \varepsilon_v}\right). \tag{29}$$

The solid/liquid interface free energy γ_{sl} can be written, by introducing Eqs. (25) and (28) into Eq. (3), as

$$\gamma_{sl} = \gamma_{sl}^0 - \Delta\gamma_0 - \Delta\gamma_{sl}^* + G_s = \gamma_{sl}^0 - \Delta\gamma_0 - \frac{2\pi\sigma^2 L_f}{\varepsilon_s}\left(\frac{\varepsilon_s - \varepsilon_l}{\varepsilon_s + \varepsilon_l}\right) - 8\pi\varepsilon_l\sigma^2 L_l\left(\frac{1}{\varepsilon_s + \varepsilon_l}\right)^2. \tag{30}$$

As a result of the irradiation, and taking into account Eqs. (29) and (30), Young's equation may be modified as

$$\gamma_{lv}(\cos\theta_0 - \cos\theta) = \frac{2\pi\sigma^2 L_f}{\varepsilon_s}\left(\frac{\varepsilon_s - \varepsilon_v}{\varepsilon_s + \varepsilon_v} - \frac{\varepsilon_s - \varepsilon_l}{\varepsilon_s + \varepsilon_l}\right) - 8\pi\varepsilon_l\sigma^2 L_l\left(\frac{1}{\varepsilon_s + \varepsilon_l}\right)^2. \tag{31}$$

The energy E^* of the interactions between the excess charge σ and its image σ^* changes the sign over a transition of a charge through an interface. The energy E^* is a continuous function of the position of the charge. Hence, for the charge located in a layer of atomic thickness, i.e., directly on the interface, the energy E^* is equal to zero.[48] In the absence of image energy, the first term in Eq. (31) is canceled and only the second term influences the wettability. In this case, Eq. (31) is transformed to

$$\gamma_{lv}(\cos\theta_0 - \cos\theta) = -8\pi\varepsilon_l\sigma^2 L_l\left(\frac{1}{\varepsilon_s + \varepsilon_l}\right)^2. \tag{32}$$

Equation (32) describes the increase of the wettability under surface charging. This result is in accordance with the results of the recent work of Chou,[49] which reports on the increase of the wettability due to the surface charge on the interface. It is clearly seen that the increase of the wettability occurs only when the excess charge σ is placed directly on the interface. In our experiments, the main influence to the wettability variation gives the charge, generated beyond the interface (Fig. 7). For this charge, as was shown above, the contribution of the G_s energy to the interface free energy may be neglected, and that results in a decrease of the wettability of the charged dielectric. In the general case [Eq. (31)], both tendencies, the decrease and the increase of the wettability, are revealed. The concluding result is dependent only on the type of excess charge distribution.

It should be mentioned that in the case of the conventional electrowetting effect, an external voltage is applied to liquid droplet, resulting in charge accumulation only at the solid/liquid interface.[3,4] In this case, the main contribution to the wettability variation is defined by the dielectric layer energy but not by the liquid double layer. However, in our case, due to the uniform charging of the interface by irradiation, the situation is the opposite, and liquid properties play a major role in wettability variation.

5. Electron irradiation induced surface potential variation

Figure 2 shows the results of the measurements of the surface potential φ_s variation using a high-resolution KPFM. It should be noted that very low fluctuations (<0.1 V) of the surface potential were observed over the scanned area ($1 \times 1\ \mu m^2$) of the irradiated SiO_2 surfaces. It is a direct evidence that almost homogeneous wettability over the SiO_2 surface is provided.

We determined the potential of the field created by the charges ρ for an explanation of our experiments (Figs. 2 and 3). It is essential to choose a right model for the surface potential calculation because of the fact that the calculations or measurements of the screening length L_f in oxide films are not reported. However, it is well known that the concentration of mobile ions in SiO_2 is very low. Most of the mobile ions precipitate on the Si/SiO_2 interface.[50–52] Few mobile ions, remained in the bulk of the dielectric films, are not able to effectively screen the field of the excess charge σ. Therefore, for our case, it is reasonable to assume that $L_f \gg h$. Thus, the model of thin films approximation should be used.

Poisson's equation is given by

$$\frac{\partial^2\varphi}{\partial x^2} = -\frac{4\pi}{\varepsilon_s}[\rho_e(x) + \rho_h(x)],$$

with boundary conditions[31] and thin film approximation,

$$\left(\frac{\partial\varphi}{\partial x}\right)_{x=0} = \frac{4\pi\sigma\varepsilon_v}{\varepsilon_s(\varepsilon_s + \varepsilon_v)},$$

$$\varphi_{x=L_d} = 0,$$

that leads to the following solution

$$\varphi(x) = \frac{4\pi\sigma(L_d - x)}{\varepsilon_s + \varepsilon_v} - \frac{4\pi}{\varepsilon_s}[\rho_e^0 R_e^2(e^{-x/R_e} - e^{-L_d/R_e}) + \rho_h^0 R_h^2(e^{-x/R_h} - e^{-L_d/R_h})].$$

The potential value at $\varphi(0)$ defines the surface band bending φ_s which is obtained by substituting $\varepsilon_v = 1$:

$$\varphi_s = \frac{4\pi\sigma L_d}{\varepsilon_s + 1} - \frac{4\pi}{\varepsilon_s}[\rho_e^0 R_e^2(1 - e^{-L_d/R_e}) + \rho_h^0 R_h^2(1 - e^{-L_d/R_h})]. \tag{33}$$

By assuming $L_d \gg R_e > R_h$, Eq. (33) is simplified to the following:

$$\varphi_s = \frac{4\pi\sigma L_d}{\varepsilon_s + 1}. \tag{34}$$

By introducing Eqs. (4)–(7) into Eq. (34), the behavior of the surface potential φ_s dependence on the E_p and Q may be explained.

C. Comparison between theory and experiment

The developed equations (6) and (33) predict the linear dependence of the surface potential φ_s on the incident charge Q in the first region, and that is consistent with the experi-

mental data (Fig. 3). Charging of dielectric materials depends on the primary electron energy E_p (Fig. 5). This dependence shows well-expressed maximum of both the decrease of the wettability and the surface potential at about $E_P^m \sim 400$ eV. The level of the decrease of the wettability is defined by the charge value and its relative distribution in the irradiated sample. The electron penetration depth R_e exceeds the hole penetration depth R_h by the free electron path λ_e before capturing by deep traps. The number of generated electrons and holes increases with growth of E_p. Thus, charging increases and, hence, enhancement of the effect of the decrease of the wettability is observed (Fig. 5). At further growth of $E_p > 400$ eV, the opposite effect plays the main role. In such a way, the electron penetration depth and the thickness of the layer, in which electron-hole pairs are generated, are enlarged. The penetration depth of holes R_h in the dielectric coincides practically with the thickness of this layer h. Thus, the relative difference between $R_e \sim R_h + \lambda_e$ and R_h decreases with the increase of the E_p value. The partial overlapping of the charges, $\rho_e(x)$ and $\rho_h(x)$, grows and then recombination of these charges becomes more probable. As a result, the density of the charges of a different sign decreases, resulting in a suppression of the effect of the decrease of the wettability. Such two opposite tendencies are capable of explaining the occurrence of the cos θ minimum as a function of E_p.

This explanation comes in good agreement with the quantitative calculation using the developed theory and the following values of parameters: $\theta_0 = 18°$, $E_{eh} = 18$ eV,[53] $\varepsilon_v = 1$, $\varepsilon_s = 3.8$,[34] $\varepsilon_l = 80.4$, $\varepsilon_{sub} = 11.7$, $\eta = 0.18$,[54] and $\gamma_{lv} = 72.8$ mJ/m^2 (for the water/vapor interface).[55] The electron penetration depth R_e was calculated using the following expression: $R_e = R_h + \lambda_e$. The λ_e value was taken to be 5 nm (Ref. 32) and the hole penetration depth R_h was assumed to be close to the maximum electron range R_m. The expression for the R_m is derived as a function of E_p:[56]

$$R_m[\text{nm}] = \frac{115(E_p[\text{keV}])^{1.35}}{\rho_g[g\ \text{cm}^{-3}]}.$$

Here, ρ_g is the density of the material. For the SiO_2, ρ_g is 2.2 g/cm^3.

Dotted lines in Fig. 5 show the results of calculations of the φ_s dependence on the E_p values [Eq. (33)]. These approximations were modeled by the use of a developed model, with $\delta(E_p)$ as a fitting parameter. The Levenberg-Marquardt method[57] was used as an iterative procedure to evaluate the best-fit values of the calculated parameters.

The experimental fitting of the secondary electron emission coefficient $\delta(E_p)$, which was determined by the estimation of $\varphi_s(E_p)$ (Fig. 5), is revealed in Fig. 8. The theoretical approximation of the secondary electron emission coefficient $\delta(E_p)$, in accordance with the theory of Lye and Dekker,[58] is plotted on the same figure (Fig. 8). The evaluated experimental dependence $\delta(E_p)$ is in good agreement with the theory[58] at $E_p > 150$ eV. At the smaller values of E_p, the theoretical values of $\delta(E_p)$ are smaller than the experimental results (Fig. 8) and coincide with the data published in Ref. 58. Maximum secondary electron emission yield and its corresponding energy were achieved at $\delta_m = 1.92$ and E_p^m

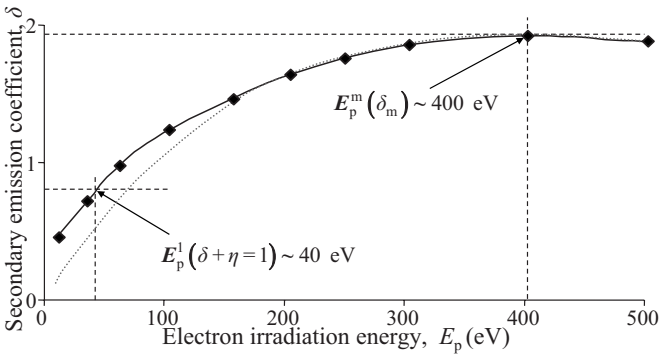

FIG. 8. Dependence of the secondary electron emission coefficient δ on the electron irradiation energy in the interval of $E_p = 10-500$ eV. The solid line refers to the experimentally values. The dotted line shows the approximation of the experimental dependence obtained in the context of the theory of Lye and Dekker (Ref. 58).

~ 400 eV, respectively. These values are consistent with the experimental measurements obtained in experiments in a rather low vacuum.[56,59] In the further calculations, we use the revealed experimental dependence of $\delta(E_p)$ (Fig. 8). The neutrality condition of the sample ($\chi = 1$) was obtained by combining the data presented on Fig. 8 and in Eq. (7), and it is carried out at $E_p^1 \sim 40$ eV. The calculated values of the minimum ($E_p^1 \sim 40$ eV) and maximum ($E_p^m \sim 400$ eV) of the effect of the decrease of the wettability are in good accordance with the data shown in Fig. 5.

The obtained experimental values of $\delta(E_p)$ were used for the calculations of the cos θ dependence on Q and E_p and the φ_s dependence on Q using the model thin film approximation [Eqs. (22) and (33)]. The nature of the observable square-law dependence of cos θ on the incident charge density Q (Fig. 3) is clear. More specifically, in accordance with Eqs. (4)–(7) and (34), the values of the charge densities, ρ_e and ρ_h, and the potential φ_s created by them increase proportionally with Q (a linear dependence) in the range of the low values of the absorbed incident electron charge (Fig. 3). Thus, the cos θ value, which is proportional to the $\Delta\gamma_{sv}^*$ and $\Delta\gamma_{sl}^*$ values [Eqs. (6) and (17)–(19)], changes as Q^2 which is consistent with experimental results (Fig. 3). The approximated curves, displayed in Figs. 3 and 5 by dotted lines, show good agreement of the developed theory with the experimental data.

In addition, the possibility of the description of the results of our experiments by the thick film approach is considered as well. When the screening length is defined as a fitting parameter, L_f is obtained close to 130 nm. Such length of L_f is related to the bulk density of mobile charges $n_f \sim 3 \times 10^{14}$ cm^{-3}, in spite of the fact that the density of positive alkali ions and protons in SiO_2 may be in the order of 10^{13} cm^{-3} or even higher.[52] However, most of these ions stay fixed at room temperature. For example, ions of H^+, Li^+, and K^+ become mobile around 400 °C,[52,60] and ions of Na^+ ~ 200 °C.[60] Therefore, the high values of n_f, essential for screening, are unachievable. This fact does not allow us to use a model of the thick film approximation for the description of our experiments.

D. Verification of the proposed model

It is known that the sample charge value σ under electron irradiation depends on a total emission coefficient χ [Eq. (7)]. Generally, the sample is negatively charged if $\chi<1$, but it has the opposite charge if $\chi>1$. There is a specific value of the primary electrons energy E_p^1 at which $\chi=1$. In this case, the sample remains uncharged ($\sigma=0$), the surface potential φ_s [Eq. (33)] should be close to zero, while the energy of the interaction between the real charge ρ and its image [Eq. (12)] is equal to zero. Thus, by neglecting the small term (G_s) of Eq. (20), the value of $\cos\theta$ is invariable ($\theta=\theta_0$) in spite of an electron irradiation. Thus, a full suppression of the effect of the decrease of the wettability is predicted at $E_p=E_p^1$. Our calculation (Fig. 8) shows that the neutrality condition of the sample ($\chi=1$) is carried out at $E_p^1\sim 40$ eV. The obtained experimental data (Fig. 5) are consistent with this estimation: the almost full suppression of the effect of the decrease of the wettability is actually observed at the incident electron energy $E_p^1\sim 40$ eV and the surface potential passes through zero for the energy close to E_p^1.

In our case, the effect of the decrease of the wettability is ascribed to the separation of the localized charges of different signs induced by an electron irradiation (first region). Such a separation may be considered as the formation of an electret state. It is known[41] that UV illumination causes a photostimulated discharge of an electret state. Therefore, one can expect that the discharge of the fabricated electret state under UV illumination should lead to a reduction of the effect of the decrease of the wettability in the first region. Such a reduction was observed in our experiments, when UV-stimulated discharge reversed the wettability of the electron-irradiated sample to the initial state.

The found electron-induced method[9] of surface free energy modification allows tailoring a high-resolution wettability patterning.[61] Figure 9 presents the electron-induced patterning of SiO_2 surface with three different levels of wettability providing sharp contrast of wetting. Open-air water microchannels were fabricated on the SiO_2 surface with different degrees of wettability, induced by variation of the incident charge density Q (the incident electron energy is $E_p=100$ eV). The patterned surface was exposed to a water vapor at a 50% RH. After cooling to a temperature of 5 °C below the dew point, the water condensed on the hydrophilic regions, producing liquid microchannels.[62] Large drops are associated with hydrophilic (untreated) region, whereas dark and bright areas, with no visible drops, are referred to the hydrophobic regions for $Q=0.10$ and 2 $\mu C/cm^2$, respectively. The tailored microchannels of 3 μm width are homogeneous and shaped as cylinder segments with a constant cross section. In this way, one should be able to produce wettability structures with a large variety of wetting morphologies.

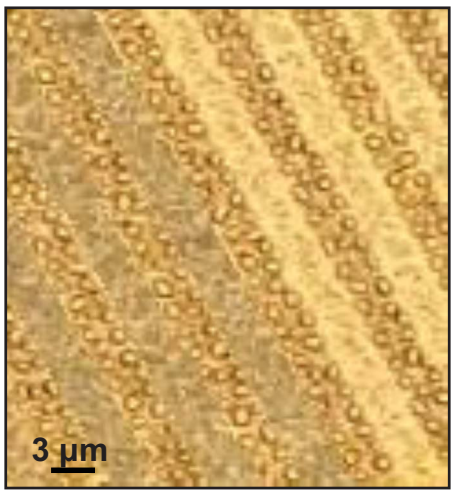

FIG. 9. (Color online) Open-air water microchannels on the SiO_2 substrate. Surface wettability patterning was performed by a low-energy electron beam irradiation with $E_p=100$ eV. Variation of the incident charge density $Q=0.10$ and 2 $\mu C/cm^2$ allows us to observe the "wettability" contrast.

The implemented study demonstrates the possibility of a controllable reduction of the wettability of a surface, resulting in tailoring of the surface free energy, using irradiation by low-energy electrons. Potential applications might be in the fields of biomedicine,[63] materials science, and microelectronic technology. Investigations of the retention of the wettability-induced SiO_2 samples show that tailored hydrophilic and hydrophobic states remained stable at least during the month under different environment conditions, such as air and water.

V. CONCLUSION

We provide experimental evidences that the electron-induced surface charge of different dielectrics leads to a pronounced decrease of the wettability. The proposed theory ascribes the observed effect at the low dose irradiation to a reduction of the solid/liquid and solid/vapor interfacial free energies and shows that the reduction of the latter is always higher. Various situations of wettability variation, for thin and thick films, induced by an electron irradiation are considered when liquid electrostatic energy contribution is taken in to consideration. The effect of the decrease of the wettability under an electron irradiation is caused only by the electrostatic energy term, related to interactions of an excess charge with its images outside the electron-irradiated dielectric film. The developed theory is in good agreement with the experimental data. The predicted suppression of the effect has been actually demonstrated under low-energy incident electron irradiation and UV illumination.

*gilr@eng.tau.ac.il

[1] G. Lippmann, Ann. Chim. Phys. **5**, 494 (1875).
[2] A. Frumkin, Actual. Sci. Ind. **373**, 5 (1936).
[3] C. Quilliet and B. Berge, Curr. Opin. Colloid Interface Sci. **6**, 34 (2001).
[4] F. Mugele and J.-C. Baret, J. Phys.: Condens. Matter **17**, R705 (2005).
[5] T. Young, Philos. Trans. R. Soc. London **95**, 65 (1805).
[6] J. A. M. Sondag-Huethorst and L. J. G. Fokkink, Langmuir **10**, 4380 (1994).
[7] W. J. J. Welters and L. J. G. Fokkink, Langmuir **14**, 1535 (1998).
[8] J. W. Gibbs, *Scientific Papers of J. W. Gibbs* (Dover, New York, 1961), Vol. 1, p. 314.
[9] G. Rosenman, D. Aronov, and Yu. Dekhtyar, PCT patent No. WO 2007/049280 (3 May 2007).
[10] D. Aronov, M. Molotskii, and G. Rosenman, Appl. Phys. Lett. **90**, 104104 (2007).
[11] D. Aronov and G. Rosenman, J. Appl. Phys. **101**, 034701 (2007).
[12] C. B. Gorman, H. A. Biebuyck, and G. M. Whitesides, Langmuir **11**, 2242 (1995).
[13] J. Lahann, S. Mitragotri, T.-N. Tran, H. Kaido, J. Sundaram, I. S. Choi, S. Hoffer, G. A. Somorjai, and R. Langer, Science **299**, 371 (2003).
[14] H. J. J. Verheijen and M. W. J. Prins, Langmuir **15**, 6616 (1999).
[15] S. L. Horswell, V. Zamlynny, H.-Q. Li, A. R. Merrill, and J. Lipkowski, Faraday Discuss. **121**, 405 (2002).
[16] S. Ray and A. K. Bhowmick, J. Appl. Polym. Sci. **83**, 2255 (2002).
[17] W. Geyer, V. Stadler, W. Eck, M. Zharnikov, A. Gölzhäuser, and M. Grunze, Appl. Phys. Lett. **75**, 2401 (1999).
[18] W. Kern and D. A. Puotinen, RCA Rev. **31**, 187 (1970).
[19] A. R. Balkenende, H. J. A. P. van de Boogaard, M. Scholten, and N. P. Willard, Langmuir **14**, 5907 (1998).
[20] C. D. Bain, E. B. Troughton, Y.-T. Tao, J. Evall, G. M. Whitesides, and R. G. Nuzzo, J. Am. Chem. Soc. **111**, 321 (1989).
[21] H. W. Fox and A. W. Zisman, J. Colloid Sci. **7**, 109 (1952).
[22] K. Seshardi, K. Froyd, A. N. Parikh, D. L. Allara, M. J. Lercel, and H. G. Craighead, J. Phys. Chem. **100**, 15900 (1996).
[23] A. B. Sieval, C. L. Huisman, A. Schonecker, F. M. Schuurmans, A. S. H. van der Heide, A. Goossens, W. C. Sinke, H. Zuilhof, and E. J. R. Sudholter, J. Phys. Chem. B **107**, 6846 (2003).
[24] A. V. Matveev, K. M. Neyman, I. V. Yudanov, and N. Rosch, Surf. Sci. **123**, 426 (1999).
[25] G. Di Valentin, A. Del Vitto, G. Pacchioniet, S. Abbet, A. S. Wörz, K. Judai, and U. Heiz, J. Phys. Chem. B **106**, 11961 (2002).
[26] A. J. A. Aquino, D. Tunega, G. Haberhauer, M. H. Gerzabek, and H. Lischka, J. Comput. Chem. **24**, 1853 (2003).
[27] P. Xiong-Skiba, D. L. Carroll, D. L. Doering, and K. H. Siek, in MRS Symposia Proceedings No. 284 (Materials Research Society, Pittsburgh, 1993), p. 275.
[28] V. A. Bakaev and W. A. Steele, J. Chem. Phys. **111**, 9803 (1999).
[29] E. A. Leed, J. O. Sofo, and C. G. Pantano, Phys. Rev. B **72**, 155427 (2005).
[30] R. R. Thomas, F. B. Kaufman, J. T. Kirleis, and R. A. Belsky, J. Electrochem. Soc. **143**, 643 (1996).
[31] J. Cazaux, J. Appl. Phys. **59**, 1418 (1986).
[32] R. Renoud, C. Attard, J.-P. Ganachaud, S. Bartholome, and A. Dubus, J. Phys.: Condens. Matter **10**, 5821 (1998).
[33] M. Touzin, D. Goeuriot, C. Goerret-Pieccourt, D. Juve, D. Treheux, and H.-J. Fitting, J. Appl. Phys. **99**, 114110 (2006).
[34] E. Schreiber and H.-J. Fitting, J. Electron Spectrosc. Relat. Phenom. **124**, 25 (2002).
[35] S. Tanuma, C. J. Powell, and D. R. Penn, Surf. Interface Anal. **17**, 927 (1991).
[36] R. C. Hughes, Phys. Rev. B **15**, 2012 (1977).
[37] K. J. Price, L. R. Sharpe, L. E. McNeil, and E. A. Irene, J. Appl. Phys. **86**, 2638 (1999).
[38] R. Williams, Phys. Rev. **140**, A569 (1965).
[39] D. J. Di Maria, in *The Physics of SiO_2 and its Interfaces*, edited by S. T. Pantelides (Pergamon, New York, 1978), pp. 160–178.
[40] F. Saigne, L. Dusseau, L. Albert, J. Fesquet, J. Gasiot, J. P. David, R. Ecoffet, R. D. Schrimpf, and K. F. Galloway, J. Appl. Phys. **82**, 4102 (1997).
[41] H. Amjadi, IEEE Trans. Dielectr. Electr. Insul. **7**, 222 (2000).
[42] P. Günther, IEEE Trans. Electr. Insul. **26**, 42 (1991).
[43] J. Rice, in *Commentary on the Scientific Writing of J. W. Gibbs*, edited by F. G. Donnan and A. Haas (Yale University Press, New Haven, 1936), Vol. 1, pp. 505–708.
[44] B. Wang and C. H. Woo, J. Appl. Phys. **94**, 4053 (2003).
[45] I. S. Gradshteyn and I. M. Ryzhik, *Table of Integrals, Series, and Products*, 5th ed. (Academic, Boston, 1994).
[46] S. R. Morrison, *Electrochemistry at Semiconductor and Oxidized Metal Electrodes* (Plenum, New York, 1980).
[47] L. Onsager and N. N. T. Samaras, J. Chem. Phys. **2**, 528 (1934).
[48] J. Cazaux, IEEE Trans. Dielectr. Electr. Insul. **3**, 75 (1996).
[49] T. Chou, Phys. Rev. Lett. **87**, 106101 (2001).
[50] R. Williams and M. H. Woods, Appl. Phys. Lett. **22**, 458 (1973).
[51] D. J. DiMaria, J. Appl. Phys. **48**, 5149 (1977).
[52] V. V. Afanasev and A. Stesmans, Phys. Rev. B **60**, 5506 (1999).
[53] G. A. Ausman, Jr. and F. B. McLean, Appl. Phys. Lett. **26**, 173 (1975).
[54] H.-J. Fitting, H. Glaefeke, and W. Wild, Phys. Status Solidi A **43**, 185 (1977).
[55] R. Aveyard and J. H. Clint, J. Chem. Soc., Faraday Trans. **93**, 1397 (1997).
[56] H. Seiler, J. Appl. Phys. **54**, R1 (1983).
[57] P. R. Gill, W. Murray, and M. H. Wright, *Practical Optimization* (Academic, London, 1981), pp. 136–137.
[58] R. G. Lye and A. J. Dekker, Phys. Rev. **107**, 977 (1957).
[59] G. F. Dionne, J. Appl. Phys. **46**, 3347 (1975).
[60] M. W. Hillen, in *The Physics of SiO_2 and Its Interfaces*, edited by S. T. Pantelides (Pergamon, New York, 1978), pp. 179–183.
[61] D. Aronov, G. Rosenmana, A. Karlov, and A. Shashkin, Appl. Phys. Lett. **88**, 163902 (2006).
[62] H. Gau, S. Herminghaus, P. Lenz, and R. Lipowsky, Science **283**, 46 (1999).
[63] D. Aronov, R. Rosen, E. Z. Ron, and G. Rosenman, Process Biochem. (Oxford, U.K.) **41**, 2367 (2006).